The Astrophysical Journal Letters, 904:L3 (8pp), 2020 November 20 https://doi.org/10.3847/2041-8213/abc564

Kozai Migration Naturally Explains the White Dwarf Planet WD1856 b

Diego J. Muñoz[1] and Cristobal Petrovich[2,3]
[1] CIERA, Northwestern University, 1800 Sherman Avenue, Evanston, IL 60208, USA
[2] Steward Observatory, University of Arizona, 933 North Cherry Avenue, Tucson, AZ 85721, USA
[3] Instituto de Astrofísica, Facultad de Física, Pontificia Universidad Católica de Chile, Casilla 306, Santiago 22, Chile
Received 2020 October 11; revised 2020 October 28; accepted 2020 October 28; published 2020 November 19

Abstract

The Jovian-sized object WD 1856 b transits a white dwarf (WD) in a compact 1.4 day orbit. Unlikely to have endured stellar evolution in its current orbit, WD 1856 b is thought to have migrated from much wider separations. Because the WD is old, and a member of a well-characterized hierarchical multiple, the well-known Kozai mechanism provides an effective migration channel for WD 1856 b. The tidal dissipation that makes this mechanism possible is sensitive to the mass of WD 1856 b, which remains unconstrained by observations. Moreover, the lack of tides in the star allows us to directly connect the current semimajor axis to the pre-migration one, from which we can infer the initial conditions of the system. By further requiring that planets must survive all previous phases of stellar evolution before migrating, we are able to constrain the main-sequence semimajor axis of WD 1856 b to have been $\sim$2.5 au, and its mass to be $\simeq$0.7–3$M_{\rm J}$. These mass limits put WD 1856 b firmly within the planet category. Furthermore, our inferred values imply that WD 1856 b was born a typical gas giant. We further estimate the occurrence rate of Kozai-migrated planets around WDs to be $\mathcal{O}(10^{-3}-10^{-4})$, suggesting that WD 1856 b is the only one in the TESS sample, but implying $\mathcal{O}(10^2)$ future detections by the LSST survey. In a sense, WD 1856 b was an ordinary Jovian planet that underwent an extraordinary dynamical history.

Unified Astronomy Thesaurus concepts: Binary stars (154); White dwarf stars (1799); Exoplanet dynamics (490); Exoplanet evolution (491); Multiple stars (1081)

1. Introduction

Recently, TESS observations revealed a planet-sized object transiting WD 1856+534, a cool, old white dwarf (WD) with an effective temperature of $T_{\rm eff} \simeq 4700$ K (Vanderburg et al. 2020). WD 1856 b has an orbital period of 1.4 d and a radius of $\simeq 10 R_\oplus$. This orbit is so compact that it is unlikely to have persisted throughout the red giant branch (RGB) and the asymptotic giant branch (AGB) phases of stellar evolution. Instead, WD 1856 b is thought to have formed at greater separations, and to have migrated inward after the main sequence (MS).

Although WD 1856 b is a cool ($<$200 K) object, its orbit resembles those of the "hot Jupiters" that accompany $\sim$1% of MS stars (e.g., Howard et al. 2012). Among the proposed mechanisms of hot Jupiter migration, the von Zeipel–Lidov–Kozai[4] (ZLK) mechanism coupled with tidal friction (Wu & Murray 2003; Fabrycky & Tremaine 2007) has emerged as a predictive and elegant contender, with several works suggesting that, at least in part, hot Jupiters inside binaries do indeed originate from this mechanism (e.g., Naoz et al. 2012; Petrovich 2015; Anderson et al. 2016).

Much like hot Jupiters, WD 1856 b could have migrated from a semimajor axis $a_{\rm p,0}$ to its current ("final") separation of $a_{\rm p,f} \approx 0.02$ au (Table 1) owing to ZLK oscillations induced by G 229-20, the known stellar companion(s) to WD 1856+534 (McCook & Sion 1999). G 229-20, a double M-dwarf, orbits WD 1856+534 at a distance of $a_{\rm out} \sim 1500$ au with an eccentricity of $\simeq$0.3, as inferred from Gaia astrometry (Vanderburg et al. 2020; see Table 1). For this stellar multiple, the timescale associated to ZLK oscillations acting on WD 1856 b is, to quadrupole level of approximation,

$$\tau_{\rm quad} \approx 4.37 \times 10^7 \left(\frac{M_{\rm WD}}{0.5 M_\odot}\right)^{1/2} \left(\frac{a_{\rm p,0}}{5{\rm au}}\right)^{-3/2} {\rm yr} \quad (1)$$

which is much shorter than the cooling age of the WD, estimated to be $\sim 6 \times 10^9$ yr (Vanderburg et al. 2020).

Despite an earlier suggestion by Agol (2011) that the ZLK mechanism could produce planets in close orbits around WDs, most theoretical efforts in this context have instead emphasized how ZLK oscillations can explain WD pollution (Hamers & Portegies Zwart 2016; Petrovich & Muñoz 2017; Stephan et al. 2017). But in addition to transporting rocky bodies, ZLK oscillations are very much capable of migrating gas giants around WDs, with the requirement that the planets survive *all* prior stages of stellar evolution.

In this work, we exploit the distinguishing feature of ZLK migration around WDs that tidal dissipation *in the host* is negligible. Therefore, once the planet is parked in a circular, tidally locked orbit, it does not decay further, in contrast to hot Jupiter systems of advanced age (e.g., Hamer & Schlaufman 2020). By relating the current semimajor axis of WD 1856 b to the maximum attainable ZLK eccentricity, we can derive the *initial* separation and the planet mass that are required for WD 1856 b to have safely migrated to its current separation while avoiding tidal disruption.

2. Eccentricity Oscillations after the MS

The triple stellar system consisting of WD 1856+534 and G 229-20 AB is hierarchical ($a_{\rm out} \gg a_{\rm AB}$; Table 1), and for our purposes, it can be considered a stellar binary (but see Section 4.3.1). The torque that this external binary exerts on the WD's close companion can trigger ZLK oscillations if the initial inclination i_0 is above some angle $i_{\rm crit}$ (39°.2 if

[4] Recently, Ito & Ohtsuka (2019) confirmed that von Zeipel (1910) carried out pioneering work on this mechanism, predating the seminal contributions of Lidov (1962) and Kozai (1962) by several decades.

Table 1
Parameters of WD 1856+534 System

WD Mass ($M_{\rm WD}$)	$0.518 \pm 0.05\,M_\odot$
WD cooling age ($T_{\rm cool}$)	5.85 ± 0.5 Gyr
Planet orbital period	1.407 days
Planet semimajor axis[a] ($a_{\rm p,f}$)	0.0204 ± 0.0012 au
Planet radius ($R_{\rm p}$)	$10.4 \pm 1\,R_\oplus$
Mass G 229-20 A (M_A)	$0.346 \pm 0.027\,M_\odot$
Mass G 229-20 B (M_B)	$0.331 \pm 0.024\,M_\odot$
$M_{\rm out} = M_A + M_B$	$0.677 \pm 0.051\,M_\odot$
A-B binary semimajor axis ($a_{\rm AB}$)	58^{+54}_{-16} au
Outer semimajor axis[b] ($a_{\rm out}$)	1500^{+700}_{-240} au
Outer eccentricity $e_{\rm out}$	$0.3^{+0.19}_{-0.1}$

Notes.
[a] Fit assumes a circular orbit (Vanderburg et al. 2020).
[b] The outer orbit refers corresponds to a Keplerian fit to the separation between WD 1856+534 and the center of mass of the G 229-20 A and B pair.

short-range forces are absent). Actual migration, however, is only possible at high inclinations, when the maximum eccentricity $e_{\rm max}$ surpasses a critical value $e_{\rm mig}$. Above $e_{\rm mig}$, the pericenter distance is only a few solar radii, which makes tidal dissipation effective. Likewise, when the eccentricity is above a critical value $e_{\rm dis} > e_{\rm mig}$, the separation at pericenter is so small that the planet can be tidally disrupted.

After successful migration, the semimajor axis is

$$a_{\rm p,f} \approx 2a_{\rm p,0}(1 - e_{\rm max}), \tag{2a}$$

subject to the condition

$$e_{\rm dis} > e_{\rm max} \geqslant e_{\rm mig}. \tag{2b}$$

Equation (2a) suggests that, if $a_{\rm p,f} \approx 0.020$ au is known (Table 1), then the original separation $a_{\rm p,0}$ can be inferred. To uniquely solve for $a_{\rm p,0}$, we must know $e_{\rm max}$ in terms of $a_{\rm p,0}$ and other parameters of the system.

2.1. Maximum Eccentricity

The maximum eccentricity $e_{\rm max}(i_0, \varepsilon_{\rm GR}, \varepsilon_{\rm Tide})$ attainable through quadrupole-order ZLK oscillations satisfies the transcendental equation

$$\frac{9}{8}\frac{1-j_{\rm min}^2}{j_{\rm min}^2}\left(j_{\rm min}^2 - \frac{5}{3}\cos^2 i_0\right) = \varepsilon_{\rm GR}\left(\frac{1}{j_{\rm min}} - 1\right) + \frac{\varepsilon_{\rm tide}}{15}\left(\frac{1 + 3e_{\rm max}^2 + \frac{3}{8}e_{\rm max}^4}{j_{\rm min}^9} - 1\right), \tag{3}$$

(Equation (50) of Liu et al. 2015) where $j_{\rm min} \equiv \sqrt{1 - e_{\rm max}^2}$ and

$$\varepsilon_{\rm GR} \equiv \frac{3\mathcal{G}M_{\rm WD}^2 a_{\rm out}^3 (1 - e_{\rm out}^2)^{3/2}}{a_{\rm p,0}^4 c^2 M_{\rm out}} \tag{4}$$

$$\varepsilon_{\rm Tide} \equiv \frac{15M_{\rm WD}^2 a_{\rm out}^3 (1 - e_{\rm out}^2)^{3/2} k_{2\rm p} R_{\rm p}^5}{a_{\rm p,0}^8 M_{\rm p} M_{\rm out}} \tag{5}$$

with $k_{2\rm p} = 0.37$ being the tidal Love number of a gas giant. The coefficients $\varepsilon_{\rm GR}$ and $\varepsilon_{\rm Tide}$ represent the strength of the short-range forces: precession due to general relativistic (GR) corrections and the planet's tidal bulge, respectively, relative to the tidal forcing by the external companion (see also Fabrycky & Tremaine 2007). These coefficients are fully determined from the system parameters (Table 1), except for the values of i_0, $a_{\rm p,0}$, and $M_{\rm p}$.

At the quadrupole-level of approximation, the value of $e_{\rm max}$ grows monotonically with i_0 until it reaches its upper bound, or "limiting eccentricity" $e_{\rm lim}$, when $\cos i_0 = 0$. Typically, $e_{\rm max}$ will not surpass the critical value $e_{\rm mig}$ unless i_0 is very close to 90°. This narrow range of inclinations, $[90° - \Delta i_{\rm quad}, 90° + \Delta i_{\rm quad}]$, subtends a solid angle $\sin \Delta i_{\rm quad}$ that equals the fraction of orbital orientations in the unit sphere that lead to migrations/disruptions (Muñoz et al. 2016).

At the octupole-level of approximation, however, an often wider range of initial inclinations can reach extreme eccentricities (Katz et al. 2011), with all angles within the "octupole window" $[90° - \Delta i_{\rm oct}, 90° + \Delta i_{\rm oct}]$, reaching $e_{\rm max} \approx e_{\rm lim}$ (Liu et al. 2015). The width of the window is

$$\Delta i_{\rm oct} \approx 2.°9\left(\frac{\varepsilon_{\rm oct}}{10^{-3}}\right)^{1/2} \tag{6}$$

(Muñoz et al. 2016) where $\varepsilon_{\rm oct} = (a_{\rm p,0}/a_{\rm out})e_{\rm out}(1 - e_{\rm out}^2)^{-1}$ is the octupole strength parameter (e.g., Ford et al. 2000; Lithwick & Naoz 2011; Naoz 2016), which vanishes for non-eccentric outer companions. For the system WD 1856 + 534/G 220-20 AB, we have $\varepsilon_{\rm oct} \approx 1.1 \times 10^{-3}(a_{\rm p,0}/5{\rm au})$. While small, this value of $\varepsilon_{\rm oct}$ is large enough to provide an octupole window of $\simeq 3°$, which covers a solid angle of $\simeq 0.05$, implying that about 5% of planets will undergo extreme eccentricity excursions.

In most cases of interest, the octupole window is wider than its quadrupole counterpart, which allows us to replace $e_{\rm max}(a_{\rm p,0}, M_{\rm p}, i_0)$ with $e_{\rm lim}(a_{\rm p,0}, M_{\rm p})$ in Equations (2), effectively relegating i_0 to a secondary role, provided that the system is inside the octupole window. By making this simplification, we reduce the number of unknowns to only two. For each $(a_{\rm p,0}, M_{\rm p})$ pair, we can compute $e_{\rm lim}$, and then derive a unique value of $a_{\rm p,f} \approx 2a_{\rm p,0}[1 - e_{\rm lim}(a_{\rm p,0}, M_{\rm p})]$. In turn, $e_{\rm lim}$ is solved from evaluating Equation (3) at $\cos i_0 = 0$:

$$0 = \frac{9}{8}e_{\rm lim}^2 - \varepsilon_{\rm GR}\left[\frac{1}{(1 - e_{\rm lim}^2)^{1/2}} - 1\right] - \frac{\varepsilon_{\rm tide}}{15}\left[\frac{1 + 3e_{\rm lim}^2 + \frac{3}{8}e_{\rm lim}^4}{(1 - e_{\rm lim}^2)^{9/2}} - 1\right]. \tag{7}$$

We illustrate this calculation in Figure 1 (left panel) for the system parameters of Table 1, and assuming $k_{\rm p} = 0.37$ and $\Delta t_L = 1$ s. In the figure, the dark blue contours show levels of constant $a_{\rm p,f}$ for different values of $a_{\rm p,0}$ and $M_{\rm p}$. The tight constraints imposed on $a_{\rm p}$ by Vanderburg et al. (2020) (gray band) translate into a tight correlation between the values of $a_{\rm p,0}$ and $M_{\rm p}$ that can explain this system.

2.2. High-e Migration within a Cooling Time

The migration condition (2b) requires explicit definitions of $e_{\rm mig}$ and $e_{\rm dis}$ (e.g., Muñoz et al. 2016). The first of these comes from the requirement that migration must be completed on timescales shorter than the cooling age of the WD. Thus, we

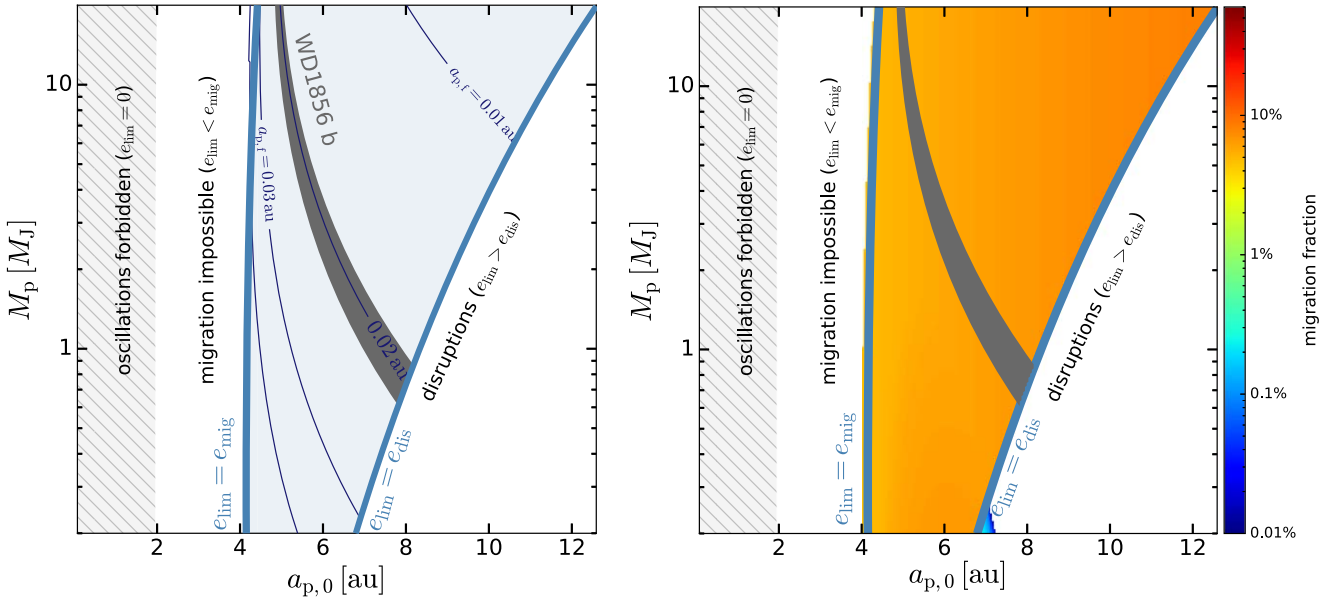

Figure 1. Kozai migration paths in the WD 1856+534 system. Left panel: region of viable migration (light-blue shading; $e_{\rm mig} < e_{\rm lim} < e_{\rm dis}$) enabled by the octupole window (Equation (6)). The thin dark blue contours depict $a_{\rm p,f}$ (Equation (2a)); the thick light-blue contours depict the boundaries of migration ($e_{\rm lim} = e_{\rm mig}$, left) and disruption ($e_{\rm lim} = e_{\rm diss}$, right) (Equation (2b)), respectively. The gray hatched region corresponds to complete quenching of ZLK oscillations due to GR ($\varepsilon_{\rm GR} \geqslant 9/8$; Equation (4)) and the dark gray region depicts the current semimajor axis of WD 1856b (Table 1). Right panel: Kozai migration fractions calculated by the analytical method of Muñoz et al. (2016). Within the migration boundaries, the migration rate is $\sim 5\%$, and is primarily given by the with of the octupole window (Equation (6)), except for a small region at small planet mass and $a_{\rm p,0} \simeq 7$, where the quadrupole window can also lead to migrations.

require $\tau_{\rm dec}^{\rm (ST)} \lesssim T_{\rm cool}$, where

$$\tau_{\rm dec}^{\rm (ST)} = \frac{0.357}{k_{\rm 2p}\Delta t_L}\frac{M_{\rm p}}{\mathcal{G}M_*^2}\frac{a_0^8\,(1-e_{\rm max})^7}{R_{\rm p}^5} \tag{8}$$

is the orbital decay timescale due to high-eccentricity excursions (e.g., Anderson et al. 2016) and where "ST" stands for the "standard tides" of weak friction theory (e.g., Alexander 1973; Hut 1981). Solving for the eccentricity, we obtain the minimum eccentricity required for migration

$$e_{\rm mig} \equiv 1 - 1.96\left(\frac{k_{\rm 2p}\Delta t_L T_{\rm cool}}{P_{\rm p,0}^2}\frac{M_{\rm WD}}{M_{\rm p}}\frac{R_{\rm p}^5}{a_{\rm p,0}^5}\right)^{1/7}. \tag{9}$$

Similarly, we define an eccentricity above which disruption takes place

$$e_{\rm dis} \equiv 1 - \eta_{\rm dis}\frac{R_{\rm p}}{a_{\rm p,0}}\left(\frac{M_{\rm WD}}{M_{\rm p}}\right)^{1/3} \tag{10}$$

where $\eta_{\rm dis} = 2.7$ (Guillochon et al. 2011).

The two limits, $e_{\rm lim} = e_{\rm mig}$ and $e_{\rm lim} = e_{\rm dis}$, are overlaid into Figure 1 (left panel) as light-blue curves. Migration is only possible within these boundaries. This additional requirement further constraints the mass and original semimajor of the WD 1856 b: $M \gtrsim 0.7 M_{\rm J}$ and 5 au $\lesssim a_{\rm p,0} \lesssim 8$ au.

The slope of the migration and disruption limits can be understood analytically. When $e_{\rm lim} \approx 1$, Equation (3) can be simplified further (see Equation (57) of Liu et al. 2015), which allows us to define "tide-dominated" and "GR-dominated" limits to $e_{\rm lim}$. Thus, when approaching the tidal disruption limit $1 - e_{\rm lim}^2 \approx (7\varepsilon_{\rm Tide}/27)^{2/9}$, for which $e_{\rm lim} = e_{\rm dis}$ implies

$$a_{\rm p,0}^{\rm (dis)} \simeq 8.4\ {\rm au}\left[\frac{a_{\rm out}\sqrt{1-e_{\rm out}^2}}{1500\ {\rm au}}\right]^{6/7}\left[\frac{\eta_{\rm dis}}{2.7}\right]^{-9/7}\left[\frac{R_{\rm p}}{R_{\rm J}}\right]^{1/7} \times \left[\frac{k_{\rm 2p}}{0.37}\right]^{2/7}\left[\frac{M_{\rm p}}{M_{\rm J}}\right]^{1/7}\left[\frac{M_{\rm WD}}{0.5M_\odot}\right]^{1/7}\left[\frac{M_{\rm out}}{0.7M_\odot}\right]^{-2/7} \tag{11}$$

Conversely, when approaching the migration limit, $1 - e_{\rm lim}^2 \approx (8\varepsilon_{\rm GR}/9)^2$, and thus, when $e_{\rm lim} = e_{\rm mig}$ we have

$$a_{\rm p}^{\rm (mig)} = 4.36\ {\rm au}\,(k_{\rm 2p}\chi\mathcal{T})^{-1/48}\left[\frac{a_{\rm out}\sqrt{1-e_{\rm out}^2}}{1500\ {\rm au}}\right]^{7/8} \times \left[\frac{R_{\rm p}}{R_{\rm J}}\right]^{-5/48}\left[\frac{M_{\rm WD}}{0.5M_\odot}\right]^{13/24}\left[\frac{M_{\rm out}}{0.7M_\odot}\right]^{-7/24}\left[\frac{M_{\rm p}}{M_{\rm J}}\right]^{1/48} \tag{12}$$

where $\chi = \Delta t_L/0.1{\rm s}$ and $\mathcal{T} = T_{\rm cool}/1{\rm Gyr}$. From these analytical expressions, we see that the dependence of $a_{\rm p}^{\rm (mig)}$ and $a_{\rm p}^{\rm (dis)}$ is weak on most parameters except for $a_{\rm out}$, which underscores the importance of having a well-characterized outer orbit when estimating the migration viability and the migration fraction.

Migration Fractions—In Figure 1 (right panel), we compute the Kozai migration fraction around WD 1856+534 following the approximated method of Muñoz et al. (2016). The figure shows that the migration fraction is vastly dominated by the octupole window (except at $a_{\rm p,0} \sim 7$ au and $M_{\rm p} \lesssim 0.2 M_{\rm J}$), which results in a fraction given by the solid angle $\sin\Delta i_{\rm oct} \approx 5\%$ regardless of planet mass and initial semimajor axis.

Final inclinations—The final inclination of the system can be estimated from the approximate conservation of $(1-e)\cos i$ as the planet eccentricity grows from $e=0$ to $e_{\rm lim}$. This inclination can be significantly larger than the naïve value of 39°.2 for systems without short-range forces (e.g., see Figure 7 in Fabrycky & Tremaine 2007). We have confirmed via time-dependent numerical integration of ZLK oscillations with tidal friction that planets that migrate from $7-9$ au to $0.02-0.04$ au end up with relative inclinations in the range 57°–123°. This range of inclinations is consistent with the relative inclination between WD 1856 b and G 229-20 AB, estimated by Vanderburg et al. (2020) to be $(67\pm11)^\circ < i < (112\pm11)^\circ$.

2.2.1. Fast Migration and Chaotic Tides

The approximate method laid out above implicitly assumes that the dissipation rate is low enough such that the energy is conserved over the ZLK timescale $\tau_{\rm quad}$, and that dissipation does not preclude $e_{\rm lim}$ from being reached. In principle, however, and under highly dissipative conditions, enough orbital energy can be lost during just one ZLK cycle to decouple the planet from the companion's tidal field, halting subsequent oscillations. This regime, referred to as "fast migration" by Petrovich (2015), can cap the maximum eccentricity to some value $e_{\rm fast}^{\rm (ST)}$ and shield planets from being tidally disrupted if $e_{\rm fast}^{\rm (ST)} < e_{\rm dis}$. In most cases, however, $e_{\rm fast}^{\rm (ST)}$ is not low enough to prevent disruption, unless unrealistically large values of Δt_L are used (Petrovich 2015).

An analogous, yet more efficient, effect can be accomplished via chaotic dynamical tides (CDT; e.g., Mardling 1995; Vick & Lai 2018; Wu 2018). In this mechanism, the planet's fundamental mode of oscillation is erratically excited/reduced at each pericenter passage. The mode can grow stochastically until it "breaks", dissipating a significant amount of energy. The CDT dissipation timescale is given by

$$\tau_{\rm dec}^{\rm (CDT)} = \pi\frac{M_{\rm p}\sqrt{\mathcal{G}M_{\rm WD}a_{\rm p,0}}}{\Delta E_\alpha}\,, \quad \Delta E_\alpha = \frac{\mathcal{G}M_{\rm p}^2}{R_{\rm p}}\eta^{-6}T_{22} \qquad (13)$$

where $\eta\equiv(a_{\rm p,0}/R_{\rm p})(M_{\rm p}/M_{\rm WD})^{1/3}(1-e)$ and ΔE_α is the amount of energy injected into the f-mode that is dissipated (e.g., Lai 1997) and T_{22} is a dimensionless function (Press & Teukolsky 1977). Using values derived by Vick et al. (2019) for a polytropic model of a gas giant, we can approximate $T_{22}\approx 2\times10^3\eta^{-10}$ for $\eta\gtrsim\eta_{\rm dis}=2.7$. The requirement for fast migration, just like in the "standard tides" case, stems from the requirement that $\tau_{\rm dec}$ is shorter than the time spent above an eccentricity e during ZLK oscillations, i.e., $\tau_{\rm dec}\lesssim\tau_{\rm quad}\sqrt{1-e_{\rm max}^2}$ (e.g., Anderson et al. 2016). Solving for the eccentricity, we find

$$e_{\rm fast}^{\rm (CDT)}\gtrsim 1-1.55\left[\left(\frac{R_{\rm p}}{a_{\rm p,0}}\right)^{15}\left(\frac{M_{\rm WD}}{M_{\rm p}}\right)^{13/3}\frac{M_{\rm WD}}{M_{\rm out}}\times\left(\frac{a_{\rm out}}{a_{\rm p,0}}\right)^3(1-e_{\rm out}^2)^{3/2}\right]^{2/31}. \qquad (14)$$

In Figure 2, we repeat the calculation leading to Figure 1, but replacing $e_{\rm lim}\rightarrow\min[e_{\rm lim}, e_{\rm fast}^{\rm (CDT)}]$. The effect of chaotic tides is readily appreciated by the dramatic shift of the disruption boundary toward much larger initial semimajor axes[5] (see Figure 10 in Vick et al. 2019), seemingly expanding the parameter space of orbits that could explain WD 1856 b (red hatched region). Within this greatly expanded parameter space, the migration condition $a_{\rm p,f}=0.02$ au (Equation (2)) constrains the planet mass within a factor of 2, but at the expense of a highly uncertain initial semimajor axis. Fortunately, the true viability of this expanded region is severely limited if we additionally require planets to have survived earlier phases of stellar evolution. Below, we show that survival during the RGB largely rules out the chaotic tide domain.

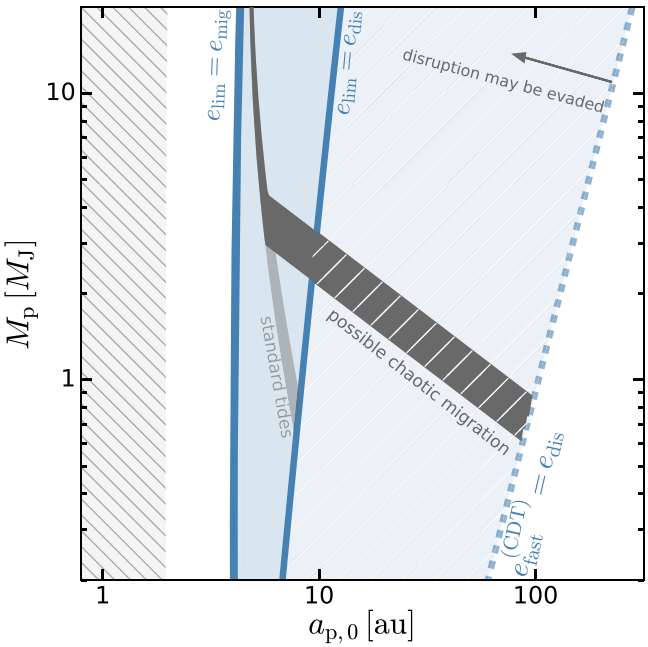

Figure 2. Same as Figure 1 (left panel), but after replacing $e_{\rm lim}$ with $\min[e_{\rm lim}, e_{\rm fast}^{\rm (CDT)}]$ (Equation (14)) to take chaotic tides into account (Section 2.2.1). The blue hatched area highlights the region in which disruption may be evaded by chaotic tides and migration is possible; this region is probabilistic, with both disruptions and migrations taking place in roughly equal fractions (Vick et al. 2019). Just as in Figure 1, the dark gray region depicts $a_{\rm p,f}=0.02$ au, corresponding to the current semimajor axis of WD 1856 b (Table 1), showing a departure from the "standard tides" result at large initial separations.

3. Pre-WD Phase

Having shown that WD 1856 b could have successfully migrated via ZLK oscillations from much larger separations, we now turn to addressing if such a planet could have orbited a WD in the first place, having survived the MS and the subsequent giant phases.

3.1. Quenched ZLK Oscillations before Mass Loss

It is known that mass loss can awaken "dormant" secular instabilities in triples and multiples. The driver behind this awakening is the unequal expansion of the orbits. For example, in the so-called "mass-loss induced eccentric Kozai" (MIEK) mechanism (Shappee & Thompson 2013), $\epsilon_{\rm oct}\propto a_{\rm p,0}/a_{\rm out}$

[5] The migration boundary on the left is also affected by chaotic tides, producing circularized orbits at greater separations (Vick et al. 2019), but this modification is of lesser relevance for objects like WD 1856 b, which lies close to the disruption boundary.

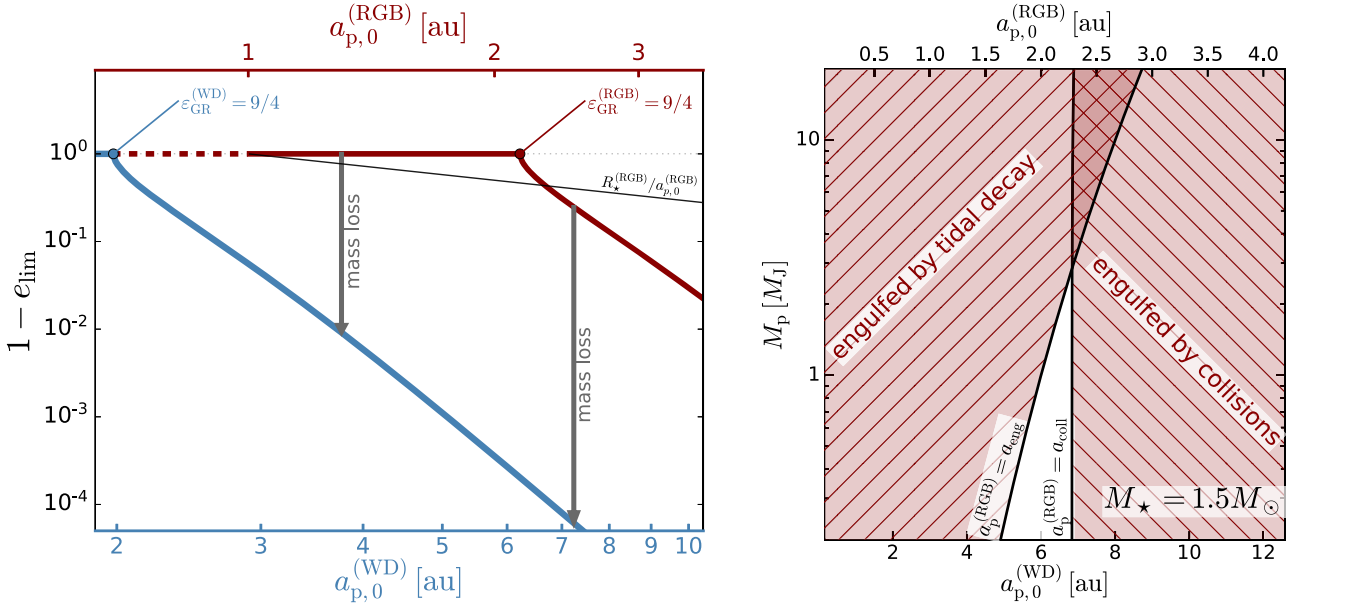

Figure 3. ZLK oscillations in the RGB phase. Left panel: modification of $e_{\rm lim}$ after a change in $\varepsilon_{\rm GR}$ triggered by mass loss between the RGB (red) and WD (blue) phases (Equation (15)). The RGB phase exhibits fully quenched ZLK for $a_{\rm p,0}^{\rm (RGB)} \lesssim 2.15$ au (when $\epsilon_{\rm GR}^{\rm (RGB)} = 9/4$); this region is awakened after a mass change of $1 M_\odot$, exposing all planets with $a_{\rm p,0}^{\rm (WD)} \gtrsim 0.68$ au to ZLK oscillations. For reference, we also depict $R_\star^{\rm (RGB)}/a_{\rm p,0}^{\rm (RGB)}$ which intersects $1 - e_{\rm lim}$ at 2.3 au (Equation (17)). Right panel: planet survival during the RGB phase. Semimajor axes greater than $a_{\rm coll} \approx 2.3$ au get too eccentric to survive collision with the inflated stellar envelope. Semimajor axes smaller than the $a_{\rm p} \propto M_{\rm p}^{1/8}$ line decay because of tides in the star (e.g., Villaver et al. 2014). The white region is the only one that survives at high inclinations.

grows, and alongside it, so does the width of the octupole window (Equation (6)), which can promote mild eccentricity oscillations into extreme ones.

Similarly, the expansion of the semimajor axes due to mass loss changes the balance of short-range forces in Equation (7). If a star of mass $M_\star$ loses an amount ΔM adiabatically[6], then the semimajor axis of the planet changes as $a_{\rm p} \to a_{\rm p} M_\star/(M_\star - \Delta M)$, while that of the binary changes as $a_{\rm out} \to a_{\rm out}(M_\star + M_{\rm out})/(M_\star + M_{\rm out} - \Delta M)$. Consequently, the GR coefficient changes by an amount

$$\varepsilon_{\rm GR} \to \varepsilon_{\rm GR} \frac{(M_\star - \Delta M)^6}{M_\star^6} \frac{(M_\star + M_{\rm out})^3}{(M_\star + M_{\rm out} - \Delta M)^3}, \quad (15)$$

which modifies the moderating or quenching effect that GR exerts on ZLK oscillations. The change in the GR coefficient is significant if we consider the mass loss rates of G, F, and A stars toward the end of their respective AGB phases. With $\Delta M \simeq 0.5{-}1.5 M_\odot$ for WD 1856+534 (Cummings et al. 2018), the respective change in $\varepsilon_{\rm GR}$ is $\simeq 0.05 - 0.003$. We further illustrate this effect in Figure 3, were we depict $e_{\rm lim}$ (Equation (7)) as a function of planet semimajor axis before and after mass loss.

3.2. Surviving the RGB Phase

The RGB phase of stellar evolution imperils any planet orbiting at a distance of a few au, compromising the planet's chances of surviving all the way to the WD phase. These planets are directly affected by the inflated stellar envelope in two ways. First, by stellar tides: the greatly expanded star makes it susceptible to planet-induced tides, which can shrink the orbit effectively, leading to engulfment if

$$a_{\rm p}^{\rm (RGB)} \leqslant a_{\rm eng} \equiv 2{\rm au}\left(\frac{M_{\rm p}}{1 M_{\rm J}}\right)^{1/8} \quad (16)$$

(e.g., Villaver et al. 2014), where $a_{\rm p}^{\rm (RGB)}$ denotes the planet semimajor axis during the RGB phase. We caution that this boundary is fuzzy and highly dependent on the tidal model (Nordhaus et al. 2010) as well as the evolution of the maximum stellar radii, especially in the late stages of the AGB evolution (e.g., Mustill & Villaver 2012; Madappatt et al. 2016).

And second, by direct high-eccentricity collisions: in the presence of a binary companion, ZLK oscillations can lead to the planet being engulfed by directly plunging it into the stellar envelope; this condition reads

$$a_{\rm p}^{\rm (RGB)} \leqslant a_{\rm coll} \equiv R_\star^{\rm (RGB)} (1 - e_{\rm lim}^{\rm (RGB)})^{-1} \quad (17)$$

where $R_\star^{\rm (RGB)} \simeq 1$ au is the maximum radius reached by the stellar envelope in the RGB phase (e.g., Villaver et al. 2014), and where $e_{\rm lim}^{\rm (RGB)}$ is the solution to Equation (7) evaluated with parameters appropriate for the RGB phase at peak radius.[7] We assume that such an encounter evaporates the planet, although we note that the complex hydrodynamical interaction with the stellar envelope may be akin to the common envelope evolution in binaries, and thus not necessarily destroy a planet/brown dwarf of sufficiently high mass (Vanderburg et al. 2020; Lagos et al. 2020).

The joint requirement $a_{\rm eng} < a_{\rm p}^{\rm (RGB)} < a_{\rm coll}$ allows the survival of planets throughout the RGB phase. As it turns out, this condition is difficult to satisfy, and a large fraction of

[6] Although assuming that mass loss is adiabatic and isotropic simplifies our calculations (e.g., $e_{\rm out}$ is preserved), one must be cautious when dealing with wide orbits (e.g., Veras et al. 2013a)

[7] For simplicity, we assume that the stellar mass at the RGB and MS phases is the same. The quality of this approximation varies significantly depending on the mass choice for the progenitor host star (see Veras 2016, Figure 3).

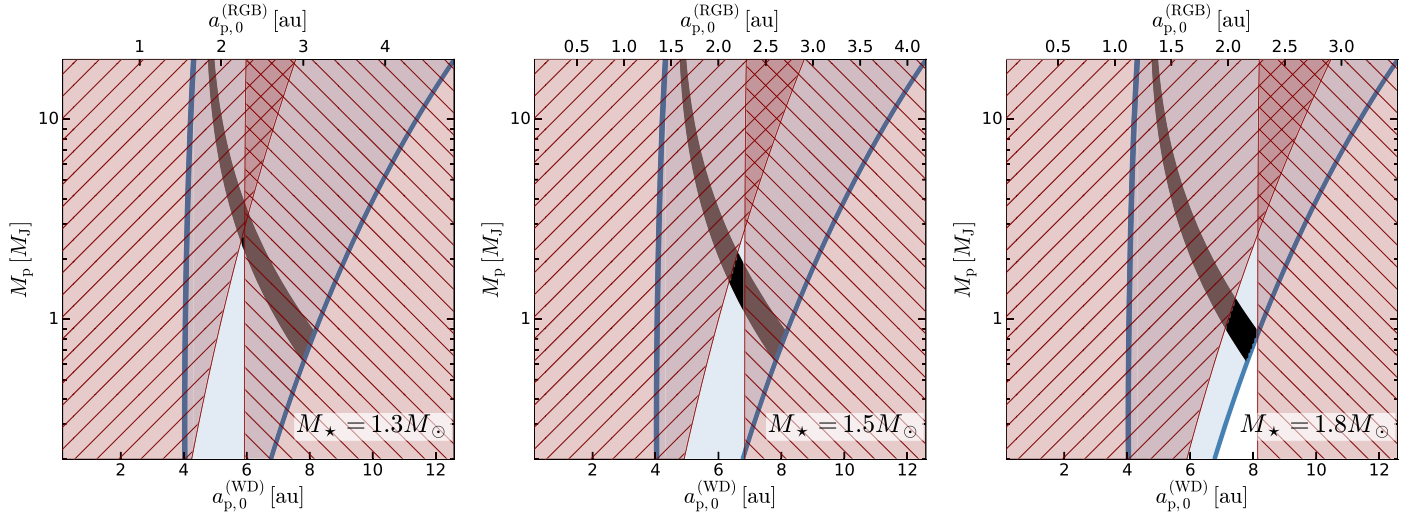

Figure 4. Survival and migration viability of highly inclined planets throughout stellar evolution. We combine the requirements Figure 1 and 3 (right panel) to constrain the initial conditions of WD 1856 b for different values of the initial stellar mass $M_\star$. The F star (left panel) does not survival and migration; the late A star (middle panel) allows for survival and migration via standard tides, the early A star (right panel) may allow for survival and migration via chaotic tides.

$a_{\rm p}^{\rm (RGB)} - M_{\rm p}$ space is excluded (Figure 3, right panel). The engulfment condition (Equation (16)) and the collision condition (Equation (17)) conspire to create a narrow region (in white) that allows inclined planets to survive.

We are now in a position to combine the migration viability conditions of Figure 1 with the survival conditions of Figure 3 (right panel), to identify which regions of parameter space give WD 1856 b a viable path to its current orbit. We show these overlaid conditions in Figure 4 for different values of the initial stellar mass $M_\star$. This figure shows that if $M_\star \leqslant 1.3 M_\odot$ (left panel) there is no possible path for WD 1856 b to have survived and migrated. Conversely, there is a narrow range of parameters that explains WD 1856 b's current orbit if $M_\star \simeq 1.5{-}1.8\,M_\odot$ (middle and right panels), which roughly corresponds to $M_{\rm p} \simeq 0.7{-}3 M_{\rm J}$ and $a_{\rm p,0} \sim 2.5$ au.

At even higher initial stellar masses, the survival region overlaps with that dominated by disruptions and/or chaotic tides (Section 2.2.1). Initial stellar masses above $1.8 M_\odot$, however, are unlikely to produce WD 1856+534 (Cummings et al. 2018), indicating that chaotic tides play a minor role, if any, in enabling planets with $a_{\rm p,0} \sim 2.5$ au to be precursors of WD 1856 b.

4. Discussion

We have demonstrated that Kozai migration can explain the recent discovery of the planet-size companion to WD 1856 +534. By simultaneously requiring that the companion is not lost prematurely during the RGB phase and that it subsequently migrates to its current location, we are able to constrain the planet's initial semimajor axis (∼2.5 au) and mass (≃0.7–3 $M_{\rm J}$).

4.1. Occurrence Rate

To provide an estimate of the occurrence rate of WD-transiting Jovians, we proceed as follows. We assume that the progenitor is always an A star. The binarity fraction of A-type stars is $\mathcal{F}_{\rm bin} \simeq 0.7$ (de Rosa et al. 2014) and their giant planet-bearing fraction is $\mathcal{F}_{\rm Jup} \simeq 0.2$ (Ghezzi et al. 2018). We assume that the semimajor axes $a_{\rm p}$ and $a_{\rm out}$, and the mutual inclination i_0 follow independent distributions. We then define the fraction of systems that survive stellar evolution and subsequently migrate into a close-in orbit as

$$\mathcal{F}_{\rm surv,mig} = \int d\log a_{\rm p} d\log a_{\rm out} d\cos i_0 \frac{dN}{d\log a_{\rm p}} \frac{dN}{d\log a_{\rm out}} \times \Theta[a_{\rm p} - 2{\rm au}] \times \Theta[(1 - e_{\rm lim}^{\rm (RGB)}) - R_\star^{\rm (RGB)}/a_{\rm p}] \times \Theta[2R_\odot/a_{\rm p}^{\rm (WD)} - (1 - e_{\rm lim}^{\rm (WD)})] \times \Theta[2.6\varepsilon_{\rm oct}^{\rm (WD)} - \cos^2 i_0], \quad (18)$$

where we have omitted the "0" subscript in $a_{\rm p,0}$ for clarity, and where Θ is the Heaviside function. The last term in the integral represents the effects of the octupole window (Equation (6)).

We evaluate $\mathcal{F}_{\rm surv,mig}$ assuming log-normal distributions in the semimajor axes: $\ln(a_{\rm p,0}/{\rm au}) \sim \mathcal{N}(0.92, 0.7)$ and $\ln(a_{\rm out}/{\rm au}) \sim \mathcal{N}(5.97, 0.78)$, in broad agreement with Fernandes et al. (2019) and de Rosa et al. (2014), respectively. For simplicity, we assume that all wide binary companions have $e_{\rm out} = 2/3$.[8] This yields $\mathcal{F}_{\rm surv,mig} \simeq 0.3\%$.

The net fraction of WDs hosting close-in Jovians owing to Kozai migration is

$$\mathcal{F}_{\rm WD,Jup} = \mathcal{F}_{\rm Jup} \times \mathcal{F}_{\rm b} \times \mathcal{F}_{\rm surv,mig} \simeq 0.2 \times 0.7 \times 0.003 \simeq 4 \times 10^{-4} \quad (19)$$

or one planet per ≃2,500 WDs, which is consistent with the 3σ upper limits of 0.45% derived from photometric surveys (Fulton et al. 2014; van Sluijs & van Eylen 2018). However, we cannot rule out other migration mechanisms that could increase $\mathcal{F}_{\rm WD,Jup}$. For example, the gas giant around WD 1145 + 017 (Gänsicke et al. 2019) is too young (∼13 Myr), and its orbital separation too wide (∼0.07 au), to be explained by Kozai migration (Veras & Fuller 2020), although the occurrence rates inferred by Gänsicke et al. (2019) are coincidentally similar to ours.

Further constraints on the occurrence of close-in Jupiters around WDs are expected in the near future from various surveys, including LSST with expected yields of 10^7 surveyed WDs

[8] Mean value for a thermal distribution, which is appropriate for wide binaries.

(Agol 2011). With a detectability of ≃2% for WD 1856b-like planets (Cortés & Kipping 2019), we expect ∼100 Kozai-migrated planets to be discovered in the the 10-year baseline of LSST.

4.2. Increasing Occurrence with Additional Effects

The main bottleneck in the low occurrence rate is the joint requirement of past survival plus a late-onset migration, which severely restricts the viable region of parameter space (Figure 4). These calculations, however, are sensitive to the choices of $a_{\rm eng}$ and $a_{\rm coll}$ (Equations (16) and (17)), as well as the disruption boundary (Equation (11)), and are thus subject to caveats.

A way of expanding the survival window (Figure 3, right panel) is to incorporate additional sources of apsidal precession to shift the $a_{\rm p}^{\rm (RGB)} = a_{\rm coll}$ boundary to the right. This effect can be accomplished by adding a planetary system interior to ∼2 au, as proposed by Petrovich & Muñoz (2017). Additional planets quench ZLK oscillations, which can be triggered once the planets are engulfed in the RGB or AGB phases (see Ronco et al. 2020 for engulfment in multi-planet systems).

4.3. Relation to Previous Work

In this work, we have used mass loss to trigger an otherwise suppressed ZLK mechanism. Delaying the onset of ZLK oscillations was instrumental for constraining the past and present properties of WD 1856 b. More generally, though, mass loss can trigger varied responses (e.g., Kratter & Perets 2012; Veras et al. 2013b), and it can lead to dynamical and secular instabilities that are effective at transporting material/minor bodies toward the WD when binaries are present (see Veras 2016 for a review).

One such possibility is the enhanced effect of galactic tides for very wide binaries (≳5000au). The galactic tide that can make $e_{\rm out}$ grow within a cooling age, thus disturbing a planetary system (Bonsor & Veras 2015). In the case of WD 1856+534, however, the outer companions are too close for the galactic tide to operate, although Vanderburg et al. (2020) did not entirely discard this mechanism due to the possible large inclination of the outer orbit respect to the Galactic plane.

A second possibility is the MIEK mechanism discussed above, which produces the widening the "octupole window", promoting conventional (quadrupolar) ZLK oscillations into extreme (octupolar) ones (Shappee & Thompson 2013; Hamers & Portegies Zwart 2016; Stephan et al. 2017). But the applicability of this mechanism is limited in the case of WD 1856 + 534, because the octupole window is known to be narrow (≃3°), even after being widened by mass loss. If planets were to be promoted into octupolar oscillations, it would be from already large inclinations, which would accompanied by large amplitude (quadrupolar) oscillations during the MS and RGB phases. Consequently, in order to survive the RGB phase, these planets would need to start from very large initial semimajor axes (∼100 au; Stephan et al. 2020). However, the scarcity of Jovians planets at large separations (Fernandes et al. 2019) renders this type of mechanism improbable.

4.3.1. Dynamics of 2 + 2 Systems

We have treated the outer M-dwarf binary as single body of mass $M_{\rm out} = M_A + M_B$. This approximation may break down in some regimes, especially when the quadrupolar field from the double M-dwarf modulates the wide binary on timescales comparable to $\tau_{\rm quad}$. Under certain conditions, the quadruple system can evolve chaotically, with the eccentricity diffusively evolving toward extreme values (Hamers & Lai 2017). In the WD 1856+534 system and $a_{\rm p,0} \simeq 5-8$ au, however, the dimensionless quantity

$$\frac{3}{4}\left(\frac{M_{\rm WD}}{M_{\rm out}}\right)^{3/2}\left(\frac{a_{\rm AB}}{a_{\rm p,0}}\right)^{3/2} \sim 10 - 28 \quad (20)$$

is too large for this chaotic diffusion to operate, and we can thus safely treat the system as a triple. It is nonetheless worthy of mention that mass loss can increase Equation (20), and conceivably activate the chaotic 2 + 2 dynamics for some systems with larger planetary semimajor axes ($a_{\rm p,0} \sim a_{\rm AB}$) after a WD is formed. This is the scenario recently explored by O'Connor et al. (2020), who concluded that, during the MS phase, WD 1856 b orbited its host at a distance of 10–20 au.

5. Conclusion

We have shown that the current orbit of WD 1856 b can be explained with Kozai migration without any ad hoc requirements other than a highly inclined orbit respect to the outer companions. By requiring that WD 1856 b survived stellar evolution and that its migration began during the WD phase, we are able to constrain its initial semimajor axis and mass. We infer an initial separation of ∼2.5 au, and a mass of $0.7-3M_{\rm J}$, implying that WD 1856 b was born a typical gas giant.

Although the initial conditions that we have inferred are consistent with the typical properties of typical exoplanetary systems, such planets ($a_{\rm p,0} <$ a few au) would rarely survive until the end of the WD phase. We predict the occurrence rate of close-in Jovians from Kozai migration around WDs to be $\mathcal{O}(10^{-3} - 10^{-4})$ and expect that the LSST survey will find ∼100 of such systems.

We thank the referee, Dimitri Veras, for a constructive report. We are grateful to Michelle Vick, Andrew Youdin, Kaitlin Kratter, María Paula Ronco, and Max Moe for useful discussions. We thank Roman Rafikov for reminding us that the current inclination between WD 1856 b and G 229-20 AB can be used as further evidence to support the Kozai migration scenario. D.J.M. acknowledges support from the CIERA Fellowship at Northwestern University and the Cottrell Fellowship Award from the Research Corporation for Science Advancement, which is partially funded by the NSF grant CHE-2039044. C.P. acknowledges support from the Bart J. Bok fellowship at Steward Observatory and ANID + REC Convocatoria Nacional subvencion a la instalacion en la Academia convocatoria 2020 grant PAI77200076.

ORCID iDs

Diego J. Muñoz https://orcid.org/0000-0003-2186-234X
Cristobal Petrovich https://orcid.org/0000-0003-0412-9314

References

Agol, E. 2011, ApJL, 731, L31
Alexander, M. E. 1973, Ap&SS, 23, 459
Anderson, K. R., Storch, N. I., & Lai, D. 2016, MNRAS, 456, 3671
Bonsor, A., & Veras, D. 2015, MNRAS, 454, 53
Cortés, J., & Kipping, D. 2019, MNRAS, 488, 1695
Cummings, J. D., Kalirai, J. S., Tremblay, P. E., Ramirez-Ruiz, E., & Choi, J. 2018, ApJ, 866, 21
de Rosa, R. J., Patience, J., Wilson, P. A., et al. 2014, MNRAS, 437, 1216
Fabrycky, D., & Tremaine, S. 2007, ApJ, 669, 1298

Fernandes, R. B., Mulders, G. D., Pascucci, I., Mordasini, C., & Emsenhuber, A. 2019, ApJ, 874, 81
Ford, E. B., Kozinsky, B., & Rasio, F. A. 2000, ApJ, 535, 385
Fulton, B. J., Tonry, J. L., Flewelling, H., et al. 2014, ApJ, 796, 114
Gänsicke, B. T., Schreiber, M. R., Toloza, O., et al. 2019, Natur, 576, 61
Ghezzi, L., Montet, B. T., & Johnson, J. A. 2018, ApJ, 860, 109
Guillochon, J., Ramirez-Ruiz, E., & Lin, D. 2011, ApJ, 732, 74
Hamer, J. H., & Schlaufman, K. C. 2020, AJ, 160, 138
Hamers, A. S., & Lai, D. 2017, MNRAS, 470, 1657
Hamers, A. S., & Portegies Zwart, S. F. 2016, MNRAS, 462, L84
Howard, A. W., Marcy, G. W., Bryson, S. T., et al. 2012, ApJS, 201, 15
Hut, P. 1981, A&A, 99, 126
Ito, T., & Ohtsuka, K. 2019, MEEP, 7, 1
Katz, B., Dong, S., & Malhotra, R. 2011, PhRvL, 107, 181101
Kozai, Y. 1962, AJ, 67, 591
Kratter, K. M., & Perets, H. B. 2012, ApJ, 753, 91
Lagos, F., Schreiber, M. R., Zorotovic, M., et al. 2020, arXiv:2010.09747
Lai, D. 1997, ApJ, 490, 847
Lidov, M. L. 1962, P&SS, 9, 719
Lithwick, Y., & Naoz, S. 2011, ApJ, 742, 94
Liu, B., Muñoz, D. J., & Lai, D. 2015, MNRAS, 447, 747
Madappatt, N., de Marco, O., & Villaver, E. 2016, MNRAS, 463, 1040
Mardling, R. A. 1995, ApJ, 450, 732
McCook, G. P., & Sion, E. M. 1999, ApJS, 121, 1
Muñoz, D. J., Lai, D., & Liu, B. 2016, MNRAS, 460, 1086
Mustill, A. J., & Villaver, E. 2012, ApJ, 761, 121
Naoz, S. 2016, ARA&A, 54, 441
Naoz, S., Farr, W. M., & Rasio, F. A. 2012, ApJL, 754, L36
Nordhaus, J., Spiegel, D. S., Ibgui, L., Goodman, J., & Burrows, A. 2010, MNRAS, 408, 631
O'Connor, C. E., Liu, B., & Lai, D. 2020, arXiv:2010.04163
Petrovich, C. 2015, ApJ, 799, 27
Petrovich, C., & Muñoz, D. J. 2017, ApJ, 834, 116
Press, W. H., & Teukolsky, S. A. 1977, ApJ, 213, 183
Ronco, M. P., Schreiber, M. R., Giuppone, C. A., et al. 2020, ApJL, 898, L23
Shappee, B. J., & Thompson, T. A. 2013, ApJ, 766, 64
Stephan, A. P., Naoz, S., & Gaudi, B. S. 2020, arXiv:2010.10534
Stephan, A. P., Naoz, S., & Zuckerman, B. 2017, ApJL, 844, L16
van Sluijs, L., & van Eylen, V. 2018, MNRAS, 474, 4603
Vanderburg, A., Rappaport, S. A., Xu, S., et al. 2020, Natur, 585, 363
Veras, D. 2016, RSOS, 3, 150571
Veras, D., & Fuller, J. 2020, MNRAS, 492, 6059
Veras, D., Hadjidemetriou, J. D., & Tout, C. A. 2013a, MNRAS, 435, 2416
Veras, D., Mustill, A. J., Bonsor, A., & Wyatt, M. C. 2013b, MNRAS, 431, 1686
Vick, M., & Lai, D. 2018, MNRAS, 476, 482
Vick, M., Lai, D., & Anderson, K. R. 2019, MNRAS, 484, 5645
Villaver, E., Livio, M., Mustill, A. J., & Siess, L. 2014, ApJ, 794, 3
von Zeipel, H. 1910, AN, 183, 345
Wu, Y. 2018, AJ, 155, 118
Wu, Y., & Murray, N. 2003, ApJ, 589, 605